HHS Public Access

Author manuscript

Adv Biol Regul. Author manuscript; available in PMC 2021 May 01.

Published in final edited form as:

Adv Biol Regul. 2020 May ; 76: 100694. doi:10.1016/j.jbior.2020.100694.

Modulation of sulfur assimilation metabolic toxicity overcomes anemia and hemochromatosis in mice

Andrew T. Hale[1], **Rachel E. Brown**[2], **Zigmund Luka**[1], **Benjamin H. Hudson**[1], **Pranathi Matta**[1], **Christopher S. Williams**[2], **John D. York**[1,*]

[1]Department of Biochemistry, Vanderbilt University School of Medicine, Nashville, TN 37232, USA

[2]Program in Cancer Biology, Vanderbilt University School of Medicine, Nashville, TN, 37232, USA

Abstract

Sulfur assimilation is an essential metabolic pathway that regulates sulfation, amino acid metabolism, nucleotide hydrolysis, and organismal homeostasis. We recently reported that mice lacking bisphosphate 3'-nucleotidase (BPNT1), a key regulator of sulfur assimilation, develop iron-deficiency anemia (IDA) and anasarca. Here we demonstrate two approaches that successfully reduce metabolic toxicity caused by loss of BPNT1: 1) dietary methionine restriction and 2) overproduction of a key transcriptional regulator hypoxia inducible factor 2α (*Hif-2a*). Reduction of methionine in the diet reverses IDA in mice lacking BPNT1, through a mechanism of downregulation of sulfur assimilation metabolic toxicity. Gaining *Hif-2a* acts through a different mechanism by restoring iron homeostatic gene expression in BPNT1 deficient mouse intestinal organoids. Finally, as loss of BPNT1 impairs expression of known genetic modifiers of iron-overload, we demonstrate that intestinal-epithelium specific loss of BPNT1 attenuates hepatic iron accumulation in mice with homozygous C282Y mutations in homeostatic iron regulator (HFE^{C282Y}), the most common cause of hemochromatosis in humans. Overall, our study uncovers genetic and dietary strategies to overcome anemia caused by defects in sulfur assimilation and identifies BPNT1 as a potential target for the treatment of hemochromatosis.

Keywords

iron deficiency anemia; hemochromatosis; iron metabolism; sulfur assimilation; nucleotide hydrolysis; methionine

*Correspondence: john.york@vanderbilt.edu.

Author contributions

A.T.H. and J.D.Y. designed research; A.T.H., R.E.B., Z.L., and B.H.H. conducted research; A.T.H., R.E.B., and C.S.W. contributed new reagents/analytic tools; A.T.H. and P.M. were responsible for animal husbandry; A.T.H., Z.L. and J.D.Y. analyzed data; and A.T.H. and J.D.Y. wrote the manuscript with input from all authors.

Introduction:

Iron homeostasis is required for numerous cellular and organismal functions. Disorders of iron homeostasis include anemia, hemochromatosis, and Parkinson's disease, among others (Hentze et al., 2010). Iron deficiency anemia (IDA) affects up to 2 billion people worldwide (Camaschella, 2015), whereas hemochromatosis is one of the most common Mendelian disorders (~1 case per 500 persons of European ancestries) and can cause organ failure due to toxic iron accumulation (Powell et al., 2016). In addition, iron buildup in the central nervous system plays a role in neurodegenerative disease (Ward et al., 2014). Thus, identifying factors involved in iron homeostasis is essential to understanding a potential basis of a wide range of diseases.

Sulfur assimilation is a critical metabolic pathway in which inorganic sulfate is incorporated into sulfur-containing amino-acids or sulfated end-products (Hudson and York, 2012; Kopriva et al., 2015; Takahashi et al., 2011). Inorganic sulfate, found in the diet of metazoans, is metabolized to 3'-phosphoadenosine 5'-phosphosulfate (PAPS) by the bifunctional enzyme phosphoadenosine phosphosulfate synthetase (PAPSS2), which harbors both ATP sulfurylase and adenosine 5'-phophosulfate (APS) kinase activities. PAPS, a high-energy intermediate and sulfate donor, serves as the substrate for several cytosolic sulfotransferases (SULTs) leading to the production of 3'-phosphoadenosine 5'-phosphate (PAP) in the cytosol. Alternatively, PAPS can be translocated into the Golgi lumen via the PAPS transporter and act as a substrate for Golgi-localized sulfotransferases (Kamiyama et al., 2003). In the cytoplasm, bisphosphate 3'-nucleotidase (Bpnt1) uses PAP as a substrate to make 5'-AMP (Spiegelberg et al., 2005; Spiegelberg et al., 1999); whereas in the Golgi, PAP is converted to 5'-AMP by the Golgi-resident PAP phosphatase (GPAPP) (Frederick et al., 2008). Loss of *Gpapp* in mice is perinatal-lethal and causes defects in chondroitin sulfation leading to chondrodysplasia (Frederick et al., 2008; Sohaskey et al., 2008). Based on studies of the *Gpapp* deficient mouse, human patients carrying loss-of-function mutations in *GPAPP* were identified, leading to characterization of a Mendelian disease (Vissers et al., 2011). Conversely, mice lacking BPNT1 develop anasarca, liver failure, and iron deficiency anemia (IDA), which are rescued in *Bpnt1* null mice harboring hypomorphic mutations in *Papss2* causing decreased PAP metabolic toxicity (Hudson et al., 2013; Hudson et al., 2018). Collectively, these studies demonstrate essential subcellular-compartment specific roles for 3'-nucleotidases in regulating sulfur assimilation and disease pathophysiology.

We extended studies of *Bpnt1* in mice through generation of an intestinal-epithelium specific mutant (*Bpnt1*$^{-/int}$) which recapitulated the profound IDA but not the other phenotypes observed in the conventional knockout (Hudson et al., 2018). We observed that *Bpnt1*$^{-/int}$ mice experienced tissue specific metabolic toxicity (elevated PAP levels in the duodenal epithelium) that cause reduced expression of key iron homeostatic genes involved in 1) dietary iron reduction via duodenal cytochrome reductase (*Cybrd1*), 2) apical iron import through divalent metal transporter 1 (*Dmt1*), 3) transcriptional coordination of iron regulatory genes by hypoxia inducible factor 2α (*Hif-2a*), and 4) iron export to the blood via ferroportin (*Fpn*). Here we further our mechanistic studies presenting two approaches to overcome metabolic toxicity resulting from BPNT1 deficiency. Remarkably, we find that simply reducing methionine in the diet of mice is sufficient to downregulate metabolic

toxicity and completely reverses IDA in *Bpnt1*$^{-/int}$ mice. Furthermore, capitalizing on the observation that loss of BPNT1 impairs expression of known genetic modifiers of hemochromatosis, the most common genetic form of iron-overload in humans, we identify inhibition of intestinal Bpnt1 as a strategy to overcome hemochromatosis in mice. Our study provides insights into the role of sulfur assimilation metabolism in mediating disorders of iron deficiency and overload in mice.

Materials and Methods

Study approval

All murine studies were approved by the Vanderbilt University Institutional Animal Care and Use Committee.

Animals and diets

Bpnt1 floxed mice (Bpnt1$^{-/fl}$) were generated as previously described (Hudson et al., 2018). Hif-2α floxed animals (Hif-2α$^{-/fl}$) were obtained from Jackson laboratories as previously described (Gruber et al., 2007). Animals expressing Cre recombinase under the control of an intestine-specific villin promoter (B6.SJL-Tg(Vil-cre)997Gum/J) were obtained from Jackson laboratories (Madison et al., 2002). All animals were maintained on standard chow unless specified. Irradiated chow containing a minimal of methionine (5CC7, 0.12% methionine) and control diet (5CC7, 0.6% methionine & 0.4% cysteine) were obtained from TestDiet (Nashville, TN). All animal care and experiments were performed in accordance with the Vanderbilt University Institutional Animal Care and Use Committee.

Enteroid culture

Primary enteroids were established as described previously (Reddy et al., 2016; Sato et al., 2009). Briefly, the first 10 cm of duodenum was removed and thoroughly flushed with ice-cold phosphate-buffered saline without calcium or magnesium (PBS) to remove luminal contents. The duodenum was then splayed open with blunt tip scissors and sequentially washed with PBS, PBS with 0.04% bleach, and PBS alone. The duodenum was minced, transferred to a fresh tube containing ice-cold PBS, and rocked at 4°C for 15 min. The duodenal fragments were then briefly vortexed, washed twice in fresh PBS and gently inverted to detach villi. After three washes, the minced duodenum was then incubated in dissociation buffer (2 mM EDTA in PBS) with gentle rocking at 4°C for 30 min. Fragments were then washed twice with fresh PBS without calcium or magnesium and placed in shaking buffer (43.3 mM sucrose and 54.9 mM sorbitol in PBS), followed my gentle shaking to manually disrupt crypts. Once the crypts were isolated, they were embedded in growth factor-reduced Matrigel (Corning, 356231) overlaid with Mouse IntestiCult media (Stem Cell Technologies, 6005). For initial plating, IntestiCult was supplemented with 1% penicillin-streptomycin and 0.002% primocin. For subsequent passages, enteroids were collected in PBS, gently sheared using a 25-G needle, and plated in fresh growth factor-reduced Matrigel overlaid with Mouse IntestiCult supplemented with 1% penicillin-streptomycin.

Full-length *Bpnt1* (*mus musculus*) was cloned into a pFUGW lentiviral mammalian expression vector containing GFP (Addgene plasmid #25870). Mutant Bpnt1 without catalytic activity (D51A) was made using a QuikChange site-directed mutagenesis kit (Agilent). Lentivirus was packaged by transfecting HEK293T cells (ATCC) at 50% confluency in 10 cm plates with 1 μg pMD2.G (Addgene plasmid #12259), 1 μg psPAX2 (Addgene plasmid #12260) vectors, and 2 μg of *Bpnt1* or $Bpnt1^{D51A}$ vector and polyethylenimine (MW 25,000, Polyscience Inc., #23966). Media was changed the following morning. Supernatant containing virus was harvested 48h later, filtered through a 0.45 μm filter, and centrifuged overnight at 4°C. Purified HIF-2α-CMV viral particles and empty-viral control were obtained from ABM (LVP479475). Viral pellets were resuspended in 250 μL L-WRN conditioned media (produced from an L-cell line engineered to secrete Wnt3a, R spondin 3, and Noggin) containing 10 μM Rock inhibitor (Y37632) and 8 μg/mL polybrene as described previously (Miyoshi and Stappenbeck, 2013). Freshly harvested crypts from $Bpnt1^{-/fl}$ and $Bpnt1^{-/int}$ mouse duodenum were resuspended in the L-WRN and viral particle solution, incubated for 6 hours, and plated in growth factor-reduced Matrigel overlaid with Intesticult supplemented with 1% penicillin-streptomycin, 0.002% primocin, and 10 μM Rock inhibitor (Y37632). Crypts were allowed to recover (and form enteroids) for 3 days before selection with 2 μg/mL puromycin to ensure positive selection of virally-transduced cells. Enteroids were then routinely split into media containing 2 μg/mL puromycin to maintain positive selection.

Quantification of PAP/PAPS levels

Quantification of PAP/PAPS was performed as previously described (Hazelton et al., 1985; Hudson et al., 2013; Hudson et al., 2018; Lin and Yang, 1998). Isolated enteroids or intestinal segments were boiled in 5 μL 50 mM glycine (pH 9.2) buffer per mg of tissue and homogenized. Lysates were centrifuged at 16,100 g and 4°C for 20 minutes. The supernatant was then added to 0.2 volumes of chloroform, thoroughly mixed and centrifuged at 16,100 g and 4°C for 20 minutes. The upper aqueous phase was collected. Quantification was performed using a colorimetric absorbance assay where Sult1a1-GST uses PAP/PAPS as a catalytic cofactor to produce 2-naphthyl sulfate from p-nitrophenyl sulfate. The byproduct of this reaction, 4-nitrophenol, is then observed over time as a marker of reaction velocity. Michaelis-Menten plots of reaction velocity vs. PAP concentration were used to determine the concentration of PAP/PAPS in the sample. PAP/PAPS concentration was then normalized to total protein content determined by Bradford assay using BSA as a standard.

Immunohistochemistry and electron microscopy

Histopathological analysis was performed on 10% formalin-fixed tissue embedded in paraffin by the Translational Pathology Shared Resource core at Vanderbilt University Medical Center. Thick sections (5 μM) were made and stained for nucleolar-resident fibrillarin (Abcam) and counterstained with DAB according to the manufacturer's suggested protocol. For transmission electron microscopy, cells and tissue fixed in buffer containing 4% paraformaldehyde, 2.5% glutaraldehyde, 2 mM $CaCl_2$ in 0.1M cacodylate pH 7.4 overnight and post-fixed in 1% tannic acid in 0.1M cacodylate for 1 hour followed by 1% OsO_4 for 1 hour. The samples were stained in 1% uranyl acetate for 30 minutes then dehydration in a graded ethanol series. After dehydration, the samples were infiltrated with a

Quetol 651 formulation of Spurr's Resin or Epon-812 using propylene oxide as a transitional solvent and polymerization at 60°C for 48 hours. Samples were thin sectioned at 70 nm and collected on 300 mesh Cu grids. Imaging was performed on an FEI T-12 transmission electron microscope equipped with a LaB6 filament at 100kv, using a AMT CCD. All electron microscopy experiments were performed using three independent mice and three independent sample preparations.

Enterocyte isolation and quantitative RT-PCR

Enterocytes were isolated as previously described (Hudson et al., 2018). Briefly, proximal duodenum (~ first 10 cm from the pyloric junction) was harvested, dissected open, and washed of luminal contents in ice-cold PBS with 1 mM PMSF. The tissue was then placed in dissociation buffer containing 1X PBS (without calcium or magnesium) containing 3 mM EDTA, 1 mM PMSF, and a protease inhibitor cocktail (Roche). Tissues maintained on a rotating apparatus at 4°C and were manually-disrupted every 10 minutes for 1 hour to slough off enterocytes. Once enterocytes had been digested from the mesenchyme, the remaining tissue was discarded, and enterocytes were pelleted by centrifugation (1000g at 4°C for 5 minutes). Cell pellets were then frozen and remained at −80°C prior to RNA isolation. RNA was extracted using a RNAeasy mini kit (Qiagen) according to manufacturer's instructions. Reverse transcription (RT) was performed using BioRad iScript reverse transcription kit. Quantitative RT-PCR was performed using SsoFast Evagreen PCR mastermix on a BioRad CFX96 machine. Primer sequences were designed using NCBI Primerblast as previously described (Hudson et al., 2018).

Hematological analysis

Hematological analysis was performed with the assistance of the Translational Pathology Shared Resource core at Vanderbilt University Medical Center. Briefly, mice were sacrificed by excess CO_2 exposure and blood was collected by cardiac puncture. Whole blood was deposited into collection tubes containing EDTA and gently mixed to avoid clot formation. Complete blood counts were performed using an Alfa Wasserman machine. Transferrin saturation was determined using a kit from Alfa Wasserman (ACl-35). Quantification of iron stores was performed as previously described (Hudson et al., 2018).

Statistics

All data are presented as mean ± SEM. Statistical significance was defined at $p< 0.05$ *a priori*. For comparisons of two groups an unpaired two-tailed student's t-test was used. For comparison of more than two groups a two-way ANOVA with Tukey's post-hoc test was used. Statistical analysis is detailed in the corresponding figure legend.

Results & Discussion:

Dietary methionine restriction reverses anemia in BPNT1 deficient mice

Bpnt1 is the mammalian orthologue of *met22*/*hal2*, and was first identified as a methionine auxotroph in budding yeast (Masselot and De Robichon-Szulmajster, 1975). However, the role of BPNT1 in methionine metabolism *in vivo* is not known. Thus, we hypothesized that dietary reduction of methionine, a major source of dietary sulfate, could modulate iron

homeostasis in BPNT1 deficient mice through one of two mechanisms: 1) improve IDA through decreased incorporation of inorganic sulfate through PAPSS2 and reduction of PAP metabolic toxicity or 2) exacerbate IDA due to a lack of substrate for the reverse reaction to make PAPS from PAP, further increasing PAP levels and exacerbate IDA. We placed mice lacking intestinal-epithelium specific *Bpnt1* ($Bpnt1^{-/int}$), which develop IDA but none of the other phenotypes observed in the global Bpnt1 knockout mice, and floxed *Bpnt1* ($Bpnt1^{-/fl}$) control mice on a methionine-restricted diet (met^{min}). After 4 weeks, we assessed duodenal PAP levels and hematological parameters. $Bpnt1^{-/int}$ mice fed met^{min} diet displayed decreased accumulation of PAP in the duodenum (Figure 1A) and normalized hematological parameters (Figure 1B–F), consistent with our first hypothesis. Thus, reduction of dietary methionine reduces PAP levels, alleviates associated metabolic toxicity and reverses IDA/iron homeostasis in $Bpnt1^{-/int}$ mice. Importantly, these results phenocopy our published forward-genetic suppression via reduced PAPSS2 function (Hudson et al., 2018), further strengthening a mechanism involving PAP metabolic toxicity. Remarkably, these data provide a simple, iron-independent dietary strategy to overcome IDA caused by loss of Bpnt1 in mice.

Catalytic activity of BPNT1 regulates iron import, sensing, and export

To gain mechanistic insights into the role of intestinal BPNT1 in iron regulation and targets of PAP-mediated metabolic toxicity, we utilized a primary mouse duodenal organoid (enteroid) culture system (Leushacke and Barker, 2014). Importantly, enteroids derived from $Bpnt1^{-/int}$ mice display elevated levels of PAP substrate (Figure 2A–B) and altered nuclear architecture, characterized by nucleolar condensation/enlargement and loss of heterochromatin as determined by immunohistochemical staining for nucleolar-resident fibrillarin and electron microscopy (Figure 2C–D), recapitulating both metabolic and histological observations due to PAP accumulation *in vivo* (Hudson et al., 2013; Hudson et al., 2018; Hudson and York, 2014). Our prior studies demonstrated that reduction of PAP synthesis through introduction of a hypomorphic mutation in PAPS synthase (*Papss2*) could suppress IDA and other phenotypes caused by a loss of BPNT1 (Hudson et al., 2013; Hudson et al., 2018). These data strongly suggested, but did not prove, that loss of BPNT1 catalytic activity, which normally converts PAP to 5'-AMP, is responsible for IDA in the BPNT1 deficient animal. To further these studies, we used lentiviral-mediated gene transfer to introduce a catalytic-dead BPNT1 mutant ($Bpnt1^{D51A}$) into enteroids isolated from $Bpnt1^{-/int}$ or *Bpnt1* floxed ($Bpnt1^{-/fl}$) control mice. We then measured mRNA expression of key iron homeostatic genes: *Cybrd1*, *Dmt1*, *Hif-2a*, and *Fpn* by quantitative real-time polymerase chain reaction (qRT-PCR) (Figure 2E). While expression of *Cybrd1, Dmt1, Hif-2a,* and *Fpn* was repressed in $Bpnt1^{-/int}$ enteroids and $Bpnt1^{-/int}$ enteroids complemented with catalytic-dead BPNT1 (-/int + $Bpnt1^{D51A}$), *Bpnt1*$^{-/int}$ enteroids complemented with wild-type Bpnt1 (-/int + $Bpnt1^{WT}$) displayed normalized iron regulatory gene expression (Figure 2E). These data demonstrate that catalytic activity of BPNT1 is required for iron homeostatic gene expression.

Restoration of Hif-2a normalizes iron homeostatic gene expression in BPNT1 deficient enteroids

Our studies indicated that PAP-mediated metabolic toxicity may act broadly to cause IDA in *Bpnt1* null mice for the following reasons: 1) PAP has been shown to interact with a number of targets (Dichtl et al., 1997; Schneider et al., 1998), 2) BPNT1 deficient mice accumulate PAP to near-equivalent levels of ADP (Hudson et al., 2013), and 3) Bpnt1$^{-/int}$ enterocytes display broad changes in gene expression, with ~25% of the transcriptome differentially expressed more than three-fold (Hudson et al., 2018). Intriguingly, Bpnt1$^{-/int}$ duodena display abnormal nucleolar-condensation/enlargement consistent with previous studies, but also display markedly decreased heterochromatin (Figure 3), consistent with massive transcriptional changes in Bpnt1$^{-/int}$ enterocytes (Hudson et al., 2018), through PAP-mediated metabolic toxicity.

While many genes were differentially expressed in Bpnt1$^{-/int}$ enterocytes, our analyses indicate that decreased *Hif-2a* transcription is a major contributing factor to IDA in Bpnt1$^{-/int}$ mice for the following reasons: 1) a statistically-significant reduction in *Hif-2a* expression in Bpnt1$^{-/int}$ enterocytes after a highly conservative Bonferroni correction for the total number of sequenced poly-A selected transcripts (Hudson et al., 2018), 2) decreased HIF-2α protein accumulation and no change in HIF-2α subcellular localization in Bpnt1$^{-/int}$ duodena (Hudson et al., 2018), 3) gene set enrichment analysis (GSEA) identified HIF-2α dependent transcription as the most significantly-enriched pathway in Bpnt1$^{-/int}$ enterocytes (Hudson et al., 2018), 4) an overlap of transcriptional signatures in enterocytes isolated from intestinal epithelium-specific *Hif-2a* knockout (Hif-2a$^{-/int}$) (Taylor et al., 2011) and Bpnt1$^{-/int}$ mice including decreased *Dmt1*, *Cybrd1*, and *Fpn* expression, and 5) Hif-2a$^{-/int}$ mice phenocopy IDA in Bpnt1$^{-/int}$ mice (Gruber et al., 2007). Thus, we reasoned that over-expression of *Hif-2a* may represent a genetic strategy to suppress loss of BPNT1 through restoration of iron homeostatic gene expression.

To test this hypothesis, we virally over-expressed *Hif-2a* or an empty vector (EV) control in Bpnt1$^{-/fl}$ and Bpnt1$^{-/int}$ enteroids, and after positive selection of stably transduced enteroids, measured *Dmt1* mRNA transcript levels by qRT-PCR. We observed *Hif-2a* overexpression elevated *Dmt1* expression in Bpnt1$^{-/fl}$ enteroids and normalized *Dmt1* expression in Bpnt1$^{-/int}$ enteroids (Figure 4A). Since apical iron import must be matched with basolateral iron efflux through ferroportin (FPN), otherwise iron would accumulate intracellularly, and *Fpn* is a direct transcriptional target of HIF-2α (Taylor et al., 2011), we speculated whether *Fpn* levels would be similarly restored with overexpression of *Hif-2a*. Indeed, overexpression of *Hif-2a* in Bpnt1$^{-/fl}$ enteroids normalized *Fpn* expression (Figure 4A). Likewise, we observe restored levels of *Cybrd1* in *Bpnt1*$^{-/int}$ enteroids complemented with Hif-2α, although *Cybrd1* appears to be dispensable for iron absorption (Gunshin et al., 2005). Collectively, our data present an intriguing genetic approach to attenuate the iron homeostatic consequences of metabolic toxicity caused by loss of BPNT1 in mice.

Of interest, prior studies in budding yeast identified 5'–3' exoribonuclease 1 (Xrn1), an inhibitor of ribosomal RNA (rRNA) processing, as a mediator of PAP toxicity due to loss of *hal2*, the yeast orthologue of *Bpnt1* (Dichtl et al., 1997). Indeed, BPNT1 deficient hepatocytes display elevation of unprocessed rRNA (5.8S "long") consistent with inhibition

of XRN1 activity (Hudson et al., 2013). Thus, we postulated that overexpression of *Xrn1* in Bpnt1$^{-/int}$ enteroids may modulate effects of PAP toxicity and restore iron homeostatic gene expression. We therefore virally overexpressed *Xrn1* in Bpnt1$^{-/int}$ and Bpnt1$^{-/fl}$ control enteroids. We observed a partial restoration of *Dmt1*, *Hif-2α*, and *Fpn* expression in Bpnt1$^{-/int}$ enteroids complemented with *Xrn1* (Figure 4B). However, nucleolar condensation/enlargement was not appreciably reversed by over-expression of *Hif-2a* or *Xrn1* in enteroids from Bpnt1$^{-/int}$ animals (Figure 5A–B). Together, our overexpression studies are consistent with both *Hif-2a*-dependent and -independent mechanisms that lead to iron-regulatory gene expression changes in Bpnt1$^{-/int}$ enteroids.

Hif-2a is epistatic to Bpnt1 in the intestinal epithelium

Since Bpnt1$^{-/int}$ and Hif-2α$^{-/int}$ mice both develop IDA and overexpression of *Hif-2a* in Bpnt1$^{-/int}$ enteroids restored iron homeostatic gene expression (Figure 4A), we aimed to interrogate the genetic interaction between *Bpnt1* and *Hif-2a in vivo*. We hypothesized that if *Bpnt1* and *Hif-2a* led to anemia via a shared pathway, then mice lacking both *Hif-2a* and *Bpnt1* would display a similar degree of anemia compared to loss of either gene alone. Conversely, if Bpnt1$^{-/int}$ mice develop IDA independent of Hif-2α, deletion of both Bpnt1 and Hif-2α would be expected to exacerbate IDA compared to deletion of either gene alone. Therefore, we generated intestine-specific Bpnt1-Hif-2α double knockout animals (Bpnt1-Hif-2α$^{-/int}$). Indeed, Bpnt1-Hif-2α$^{-/int}$ mice display nearly identical hematological parameters (hemoglobin, mean corpuscular volume, and transferrin saturation) compared to Bpnt1$^{-/int}$ mice (Figure 6A–C). In addition, transcriptional targets of Hif-2α, *Dmt1* and *Fpn*, were equally repressed in enterocytes isolated from Bpnt1$^{-/int}$ and Bpnt1-Hif-2α$^{-/int}$ mice (Figure 6D–F). However, it should be noted that the degree of anemia in Bpnt1$^{-/int}$ mice was more severe than in Hif-2α$^{-/int}$ mice (Figure 6A–C). These data suggest that *Hif-2a* is epistatic to *Bpnt1* in the intestine; however, these data also support the conclusion that *Hif-2a*-independent mechanisms also contribute to IDA in Bpnt1$^{-/int}$ mice.

Intestinal-epithelium specific loss of Bpnt1 attenuates hepatic iron-overload in Hfe^{C282Y} mice

The current treatment for hemochromatosis is phlebotomy, which is effective in many cases, but a targeted pharmacological approach to treat hemochromatosis would reduce morbidity and improve quality of life (Powell et al., 2016). Intriguingly, pharmacological inhibition of HIF-2α has been shown to abrogate exogenous iron-overload in mice (Schwartz et al., 2019). Furthermore, DMT1 function mitigates iron-overload in mice with homozygous C282Y mutations in homeostatic iron regulator (Hfe^{C282Y}) (Levy et al., 2000), the most common genetic cause of hemochromatosis in humans. Since Bpnt1$^{-/int}$ mice display impaired *Dmt1* and *Hif-2a* expression, we hypothesized that loss of Bpnt1 may be protective against iron-overload. Thus, we crossed intestinal-specific, Bpnt1 floxed (Bpnt1$^{-/fl}$) mice with global Hfe^{C282Y} mice to obtain Bpnt1$^{-/int}$-Hfe^{C282Y} experimental animals. Analysis of hepatic iron levels revealed a ~50% reduction in hepatic iron stores in Bpnt1$^{-/int}$ mice, whereas Hfe^{C282Y} mice displayed ~2-fold elevation in hepatic iron (Figure 7A–B). Remarkably, Bpnt1$^{-/int}$-Hfe^{C282Y} mice displayed normalized hepatic-iron content, but display decreased hemoglobin, mean corpuscular volume, total iron binding capacity, and transferrin saturation compared to control animals (Figure 7A–F). Overall, these data

suggest that inhibition of intestinal Bpnt1 may be an attractive strategy to treat hemochromatosis.

Targeting Bpnt1 may have several advantages over pharmacological inhibition of DMT1 or HIF-2α. Blocking apical iron import through DMT1 may reduce iron absorption, but also inhibit uptake of other divalent metals (Picard et al., 2000). While loss of *Bpnt1* impairs DMT1 expression and response to iron deficiency (Hudson et al., 2018), Bpnt1 mutant mice do not display any signs of divalent metal deficiency (seizures, muscle spasms, pernicious anemia etc.) at any age. Furthermore, while nearly ~90% of mice harboring loss of function mutations in *Dmt1* die before weaning (Russell et al., 1970), $Bpnt1^{-/int}$ mice display normal lifespan (Hudson et al., 2018). While HIF-2α inhibitors have been developed, they present many challenges due to HIF-2α's complex post-translational regulatory mechanisms, interaction with transcriptional coactivators, and nuclear localization (Wigerup et al., 2016). Conversely, loss of BPNT1 impairs *Hif-2a* mRNA and protein levels (Fig. 2A and (Hudson et al., 2018)), achieving the functional benefits of direct pharmacological inhibition. Our data suggests that inhibition of BPNT1 catalytic activity, leading to select metabolic accumulation in the intestine, may be beneficial for the treatment of hemochromatosis.

Our study reveals an unexpected genetic mechanism, via loss of intestinal *Bpnt1*, to attenuate hepatic iron accumulation in mice harboring biallelic Hfe^{C282Y} mutations, the most common genetic cause of hemochromatosis in humans. These data suggest that inhibition of intestinal Bpnt1 may represent an improved pharmacologic approach to treat hemochromatosis and other disorders of iron overload, possibly with minimal side effects. Importantly, we provide the first evidence that dietary changes in methionine, and a major source of sulfate, are able to rescue disease phenotypes associated with loss of BPNT1 and resulting metabolic toxicity due to PAP accumulation. These data are consistent with a mechanism by which incorporation of inorganic sulfate is a rate-limiting step in sulfur assimilation. Furthermore, based on the unique phenotype of *Bpnt1* deficient mice (severe IDA, anasarca, and liver failure), targeted sequencing of *Bpnt1* may be warranted in patients with individual or combined phenotypes whose pathophysiologies do not map to known genetic lesions. Finally, as BPNT1 is inhibited at therapeutic levels of lithium and mediates lithium-induced toxicity in a variety of organisms (Meisel and Kim, 2016; Spiegelberg et al., 2005; Spiegelberg et al., 1999), these data may represent potential strategies to overcome side effects associated with lithium therapy that may be caused by PAP accumulation.

Acknowledgements

This work was supported by the National Institutes of Health grants to A.T.H. (F30HL143826, 5T32GM007347), R.E.B. (F30DK120149, 5T32GM007347), C.S.W. (R01DK099204) and J.D.Y. (R01GM124404). C.S.W. is also supported by the Office of Medical Research, Department of Veteran Affairs (1I01BX001426). This work was also supported by funds from the Vanderbilt University School of Medicine and the Natalie Overall Warren Professorship (both to J.D.Y).

References

Camaschella C, 2015 Iron-deficiency anemia. N Engl J Med 372(19), 1832–1843. [PubMed: 25946282]

Dichtl B, Stevens A, Tollervey D, 1997 Lithium toxicity in yeast is due to the inhibition of RNA processing enzymes. Embo j 16(23), 7184–7195. [PubMed: 9384595]

Frederick JP, Tafari AT, Wu SM, Megosh LC, Chiou ST, Irving RP, York JD, 2008 A role for a lithium-inhibited Golgi nucleotidase in skeletal development and sulfation. Proc Natl Acad Sci U S A 105(33), 11605–11612. [PubMed: 18695242]

Gruber M, Hu CJ, Johnson RS, Brown EJ, Keith B, Simon MC, 2007 Acute postnatal ablation of Hif-2alpha results in anemia. Proc Natl Acad Sci U S A 104(7), 2301–2306. [PubMed: 17284606]

Gunshin H, Starr CN, Direnzo C, Fleming MD, Jin J, Greer EL, Sellers VM, Galica SM, Andrews NC, 2005 Cybrd1 (duodenal cytochrome b) is not necessary for dietary iron absorption in mice. Blood 106(8), 2879–2883. [PubMed: 15961514]

Hazelton GA, Hjelle JJ, Dills RL, Klaassen CD, 1985 A radiometric method for the measurement of adenosine 3'-phosphate 5'-phosphosulfate in rat and mouse liver. Drug Metab Dispos 13(1), 30–34. [PubMed: 2858373]

Hentze MW, Muckenthaler MU, Galy B, Camaschella C, 2010 Two to tango: regulation of Mammalian iron metabolism. Cell 142(1), 24–38. [PubMed: 20603012]

Hudson BH, Frederick JP, Drake LY, Megosh LC, Irving RP, York JD, 2013 Role for cytoplasmic nucleotide hydrolysis in hepatic function and protein synthesis. Proc Natl Acad Sci U S A 110(13), 5040–5045. [PubMed: 23479625]

Hudson BH, Hale AT, Irving RP, Li S, York JD, 2018 Modulation of intestinal sulfur assimilation metabolism regulates iron homeostasis. Proc Natl Acad Sci U S A 115(12), 3000–3005. [PubMed: 29507250]

Hudson BH, York JD, 2012 Roles for nucleotide phosphatases in sulfate assimilation and skeletal disease. Adv Biol Regul 52(1), 229–238. [PubMed: 22100882]

Hudson BH, York JD, 2014 Tissue-specific regulation of 3'-nucleotide hydrolysis and nucleolar architecture. Adv Biol Regul 54, 208–213. [PubMed: 24309248]

Kamiyama S, Suda T, Ueda R, Suzuki M, Okubo R, Kikuchi N, Chiba Y, Goto S, Toyoda H, Saigo K, Watanabe M, Narimatsu H, Jigami Y, Nishihara S, 2003 Molecular cloning and identification of 3'-phosphoadenosine 5'-phosphosulfate transporter. The Journal of biological chemistry 278(28), 25958–25963. [PubMed: 12716889]

Kopriva S, Talukdar D, Takahashi H, Hell R, Sirko A, D'Souza SF, Talukdar T, 2015 Editorial: Frontiers of Sulfur Metabolism in Plant Growth, Development, and Stress Response. Front Plant Sci 6, 1220. [PubMed: 26793206]

Leushacke M, Barker N, 2014 Ex vivo culture of the intestinal epithelium: strategies and applications. Gut 63(8), 1345–1354. [PubMed: 24841573]

Levy JE, Montross LK, Andrews NC, 2000 Genes that modify the hemochromatosis phenotype in mice. J Clin Invest 105(9), 1209–1216. [PubMed: 10791995]

Lin ES, Yang YS, 1998 Colorimetric determination of the purity of 3'-phospho adenosine 5'-phosphosulfate and natural abundance of 3'-phospho adenosine 5'-phosphate at picomole quantities. Anal Biochem 264(1), 111–117. [PubMed: 9784194]

Madison BB, Dunbar L, Qiao XT, Braunstein K, Braunstein E, Gumucio DL, 2002 Cis elements of the villin gene control expression in restricted domains of the vertical (crypt) and horizontal (duodenum, cecum) axes of the intestine. The Journal of biological chemistry 277(36), 33275–33283. [PubMed: 12065599]

Masselot M, De Robichon-Szulmajster H, 1975 Methionine biosynthesis in Saccharomyces cerevisiae. I. Genetical analysis of auxotrophic mutants. Molecular & general genetics : MGG 139(2), 121–132. [PubMed: 1101032]

Meisel JD, Kim DH, 2016 Inhibition of Lithium-Sensitive Phosphatase BPNT-1 Causes Selective Neuronal Dysfunction in C. elegans. Curr Biol 26(14), 1922–1928. [PubMed: 27397889]

Miyoshi H, Stappenbeck TS, 2013 In vitro expansion and genetic modification of gastrointestinal stem cells in spheroid culture. Nature protocols 8, 2471. [PubMed: 24232249]

Picard V, Govoni G, Jabado N, Gros P, 2000 Nramp 2 (DCT1/DMT1) expressed at the plasma membrane transports iron and other divalent cations into a calcein-accessible cytoplasmic pool. The Journal of biological chemistry 275(46), 35738–35745. [PubMed: 10942769]

Powell LW, Seckington RC, Deugnier Y, 2016 Haemochromatosis. Lancet 388(10045), 706–716. [PubMed: 26975792]

Reddy VK, Short SP, Barrett CW, Mittal MK, Keating CE, Thompson JJ, Harris EI, Revetta F, Bader DM, Brand T, Washington MK, Williams CS, 2016 BVES Regulates Intestinal Stem Cell Programs and Intestinal Crypt Viability after Radiation. Stem cells (Dayton, Ohio) 34(6), 1626–1636.

Russell ES, McFarland EC, Kent EL, 1970 Low viability, skin lesions, and reduced fertility associated with microcytic anemia in the mouse. Transplantation proceedings 2(1), 144–151. [PubMed: 5521744]

Sato T, Vries RG, Snippert HJ, van de Wetering M, Barker N, Stange DE, van Es JH, Abo A, Kujala P, Peters PJ, Clevers H, 2009 Single Lgr5 stem cells build crypt-villus structures in vitro without a mesenchymal niche. Nature 459(7244), 262–265. [PubMed: 19329995]

Schneider B, Xu YW, Janin J, Veron M, Deville-Bonne D, 1998 3'-Phosphorylated nucleotides are tight binding inhibitors of nucleoside diphosphate kinase activity. The Journal of biological chemistry 273(44), 28773–28778. [PubMed: 9786875]

Schwartz AJ, Das NK, Ramakrishnan SK, Jain C, Jurkovic MT, Wu J, Nemeth E, Lakhal-Littleton S, Colacino JA, Shah YM, 2019 Hepatic hepcidin/intestinal HIF-2alpha axis maintains iron absorption during iron deficiency and overload. J Clin Invest 129(1), 336–348. [PubMed: 30352047]

Sohaskey ML, Yu J, Diaz MA, Plaas AH, Harland RM, 2008 JAWS coordinates chondrogenesis and synovial joint positioning. Development 135(13), 2215–2220. [PubMed: 18539921]

Spiegelberg BD, Dela Cruz J, Law TH, York JD, 2005 Alteration of lithium pharmacology through manipulation of phosphoadenosine phosphate metabolism. The Journal of biological chemistry 280(7), 5400–5405. [PubMed: 15583009]

Spiegelberg BD, Xiong JP, Smith JJ, Gu RF, York JD, 1999 Cloning and characterization of a mammalian lithium-sensitive bisphosphate 3'-nucleotidase inhibited by inositol 1,4-bisphosphate. The Journal of biological chemistry 274(19), 13619–13628. [PubMed: 10224133]

Takahashi H, Kopriva S, Giordano M, Saito K, Hell R, 2011 Sulfur assimilation in photosynthetic organisms: molecular functions and regulations of transporters and assimilatory enzymes. Annu Rev Plant Biol 62, 157–184. [PubMed: 21370978]

Taylor M, Qu A, Anderson ER, Matsubara T, Martin A, Gonzalez FJ, Shah YM, 2011 Hypoxia-inducible factor-2alpha mediates the adaptive increase of intestinal ferroportin during iron deficiency in mice. Gastroenterology 140(7), 2044–2055. [PubMed: 21419768]

Vissers LE, Lausch E, Unger S, Campos-Xavier AB, Gilissen C, Rossi A, Del Rosario M, Venselaar H, Knoll U, Nampoothiri S, Nair M, Spranger J, Brunner HG, Bonafe L, Veltman JA, Zabel B, Superti-Furga A, 2011 Chondrodysplasia and abnormal joint development associated with mutations in IMPAD1, encoding the Golgi-resident nucleotide phosphatase, gPAPP. Am J Hum Genet 88(5), 608–615. [PubMed: 21549340]

Ward RJ, Zucca FA, Duyn JH, Crichton RR, Zecca L, 2014 The role of iron in brain ageing and neurodegenerative disorders. The Lancet. Neurology 13(10), 1045–1060. [PubMed: 25231526]

Wigerup C, Pahlman S, Bexell D, 2016 Therapeutic targeting of hypoxia and hypoxia-inducible factors in cancer. Pharmacology & therapeutics 164, 152–169. [PubMed: 27139518]

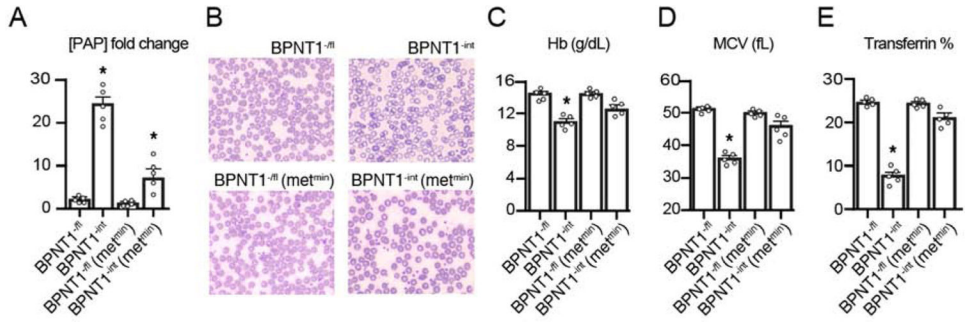

Figure 1.

Dietary methionine restriction reduces metabolic toxicity and reverses iron deficiency anemia in Bpnt1$^{-/int}$ mice. (A) PAP levels in duodena isolated from Bpnt1$^{-/fl}$ and Bpnt1$^{-/int}$ mice fed standard chow (-/fl and -/int, respectively) or a minimal-methionine chow (met^{min}) for 4 weeks (n= 5). (B) Representative image of Wright-Giemsa stained blood-smear from Bpnt1$^{-/fl}$ fed standard chow (-/fl), Bpnt1$^{-/int}$ fed standard chow (-/int), Bpnt1$^{-/fl}$ fed minimal-methionine chow (-/fl met^{min}), and Bpnt1$^{-/int}$ fed minimal-methionine chow (-/int met^{min}). (C) Hemoglobin (Hb, g/dL), (D) mean corpuscular volume (MCV, fL), and (E) Transferrin saturation (transferrin %) (n= 5). *Represents $p < 0.05$ by two-way ANOVA with Tukey's post-hoc test. Data are represented as mean ± SEM. There were no statistically-significant differences in any parameter tested between male and female mice.

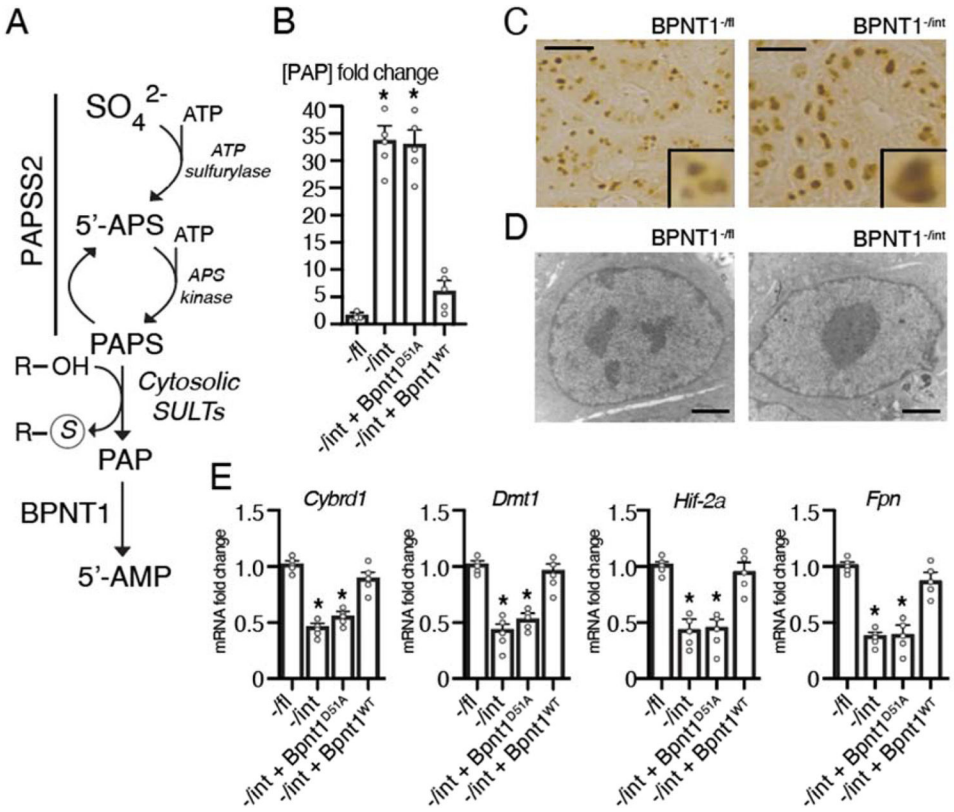

Figure 2.

(A) Abbreviated components of the evolutionarily-conserved cytosolic sulfur assimilation pathway. Inorganic sulfate (SO_4^{2-}) obtained from the diet or turnover of amino acids is incorporated by the action of the bifunctional enzyme 3'-phosphoadenosine 5-phosphosulfate synthase 2 (Papss2), a bifunctional enzyme, which acts as an ATP sulfurylase to generate adenosine 5'-phosphosulfate (5'-APS) and as an 5'-APS kinase to generate 3'-phosphoadenosine 5'-phosphosulfate (PAPS). A number of cytosolic sulfotransferases (SULTs) use PAPS as a sulfur-donor to sulfate target proteins, generating 3'-phosphoadenosine 5'-phosphate (PAP). Bisphosphate 3'-nucleotidase (Bpnt1) then catalyzes the terminal step of cytosolic sulfur assimilation to produce adenosine 5'-phosphate (5'-AMP) using PAP as a substrate. (B) Quantification of PAP levels in $Bpnt1^{-/fl}$ floxed control (-/fl), villin-cre driven knockout of Bpnt1 (-/int) and -/int duodenal enteroids (n=5). *Represents $p < 0.05$ by two-tailed student's t-test. (C) Representative image of nucleolar-resident fibrillarin staining demonstrating in $Bpnt1^{-fl}$ (left) and $Bpnt1^{-/int}$ (right) enteroids. Scale bar represents 10 μm. Inset is representative enteroid. (D) Representative transmission electron microscopy image in $Bpnt1^{-/fl}$ and $Bpnt1^{-/int}$ enteroids taken at 11,000x magnification. Scale bar represents 2 microns. (E) qRT-PCR of *Cybrd1*, *Dmt1*, *Hif-2α,* or *Fpn* relative to β-actin from complemented enteroid lines (n=5) described in (B). *Represents $p < 0.05$ by two-way ANOVA with Tukey's post-hoc test. Data are represented as mean ± SEM.

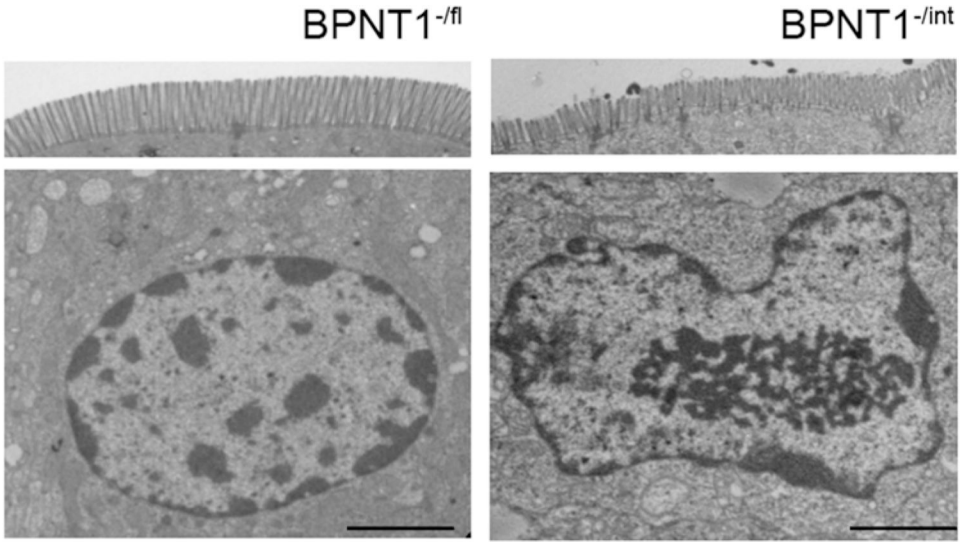

Figure 3.

Bpnt1$^{-/int}$ mice display decreased heterochromatin, abnormal brush border architecture, and nucleolar condensation. Representative transmission electron micrograph of brush border (top) and enterocyte (bottom) from duodena isolated from Bpnt1$^{-/fl}$ (-/fl) and Bpnt1$^{-/int}$ (-/int) mice. Scale bars represent 2 μm. 3,200x magnification. All experiments were performed in triplicate.

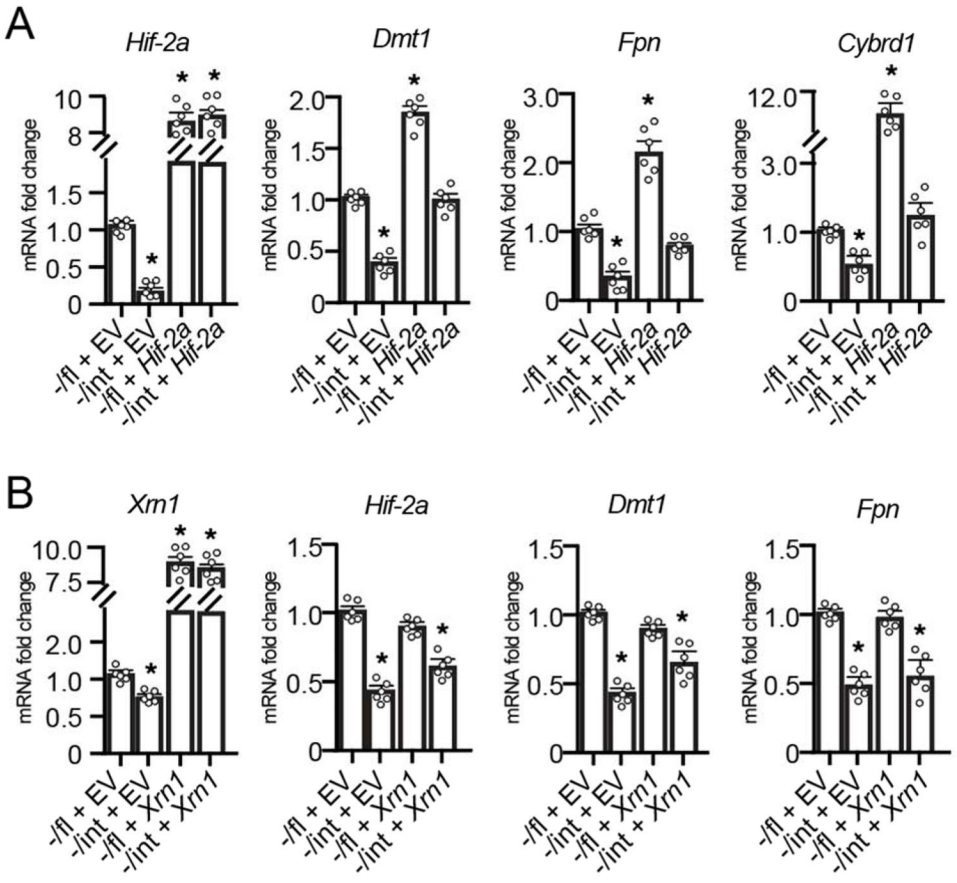

Figure 4.

Restoration of Hif-2α, but not Xrn1, normalizes iron-regulatory gene expression perturbations in Bpnt1$^{-/int}$ enteroids. qRT-PCR of *HIF-2α*, *Dmt1*, *Fpn*, and *Cybrd1* from enteroids isolated from Bpnt1$^{-/fl}$ (-/fl) or Bpnt1$^{-/int}$ (-/int) mice and infected with empty vector (EV) control or a lentivirus expressing mouse Hif-2α (A) or mouse Xrn1 (B). *Represents $p < 0.05$ by two-way ANOVA with Tukey's post-hoc test. Data are represented as mean ± SEM. There were no statistically-significant differences in any parameter tested between male and female mice.

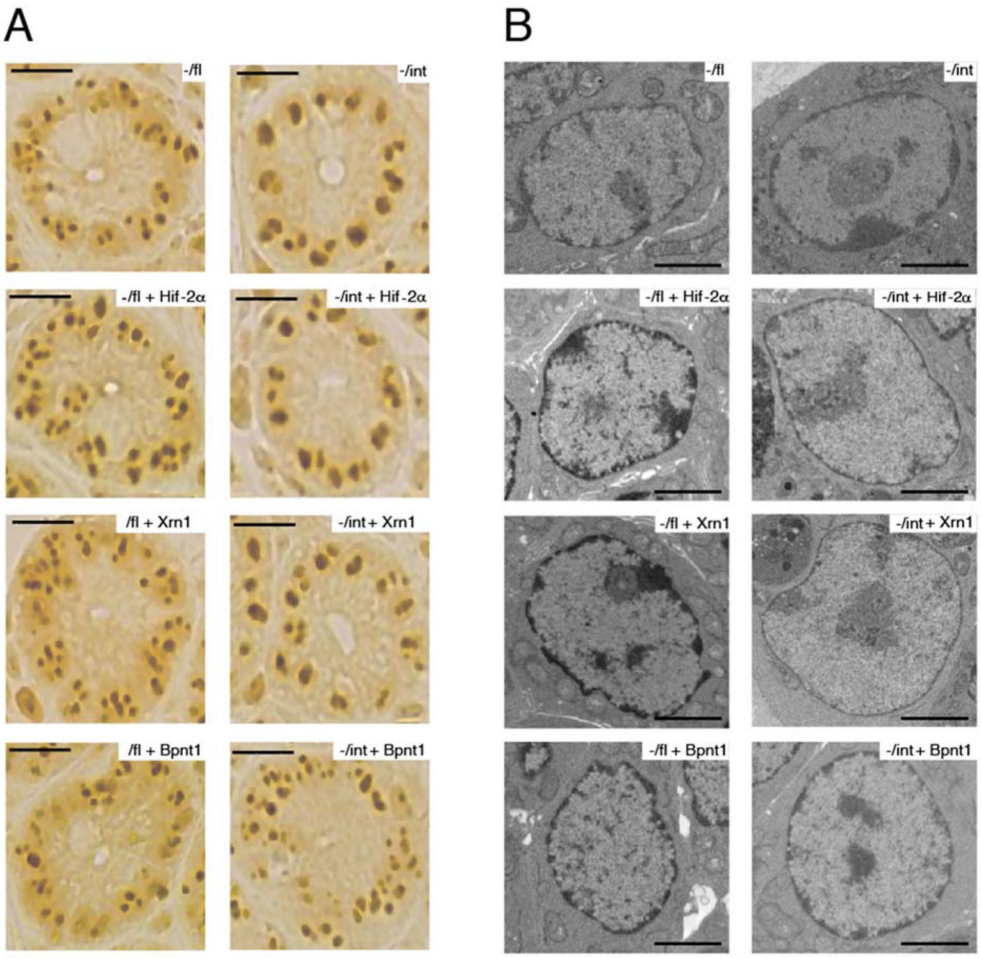

Figure 5.

(A) Representative images of fibrillarin-stained enteroids as described in (A-B). Scale bar represents 10 μm. (B) Representative transmission electron microscopy images of -/fl and -/int enteroids complemented with Hif-2α, Xrn1 or Bpnt1 taken at 4,400x magnification. Scale bar represents 2 μm. All experiments were performed in triplicate.

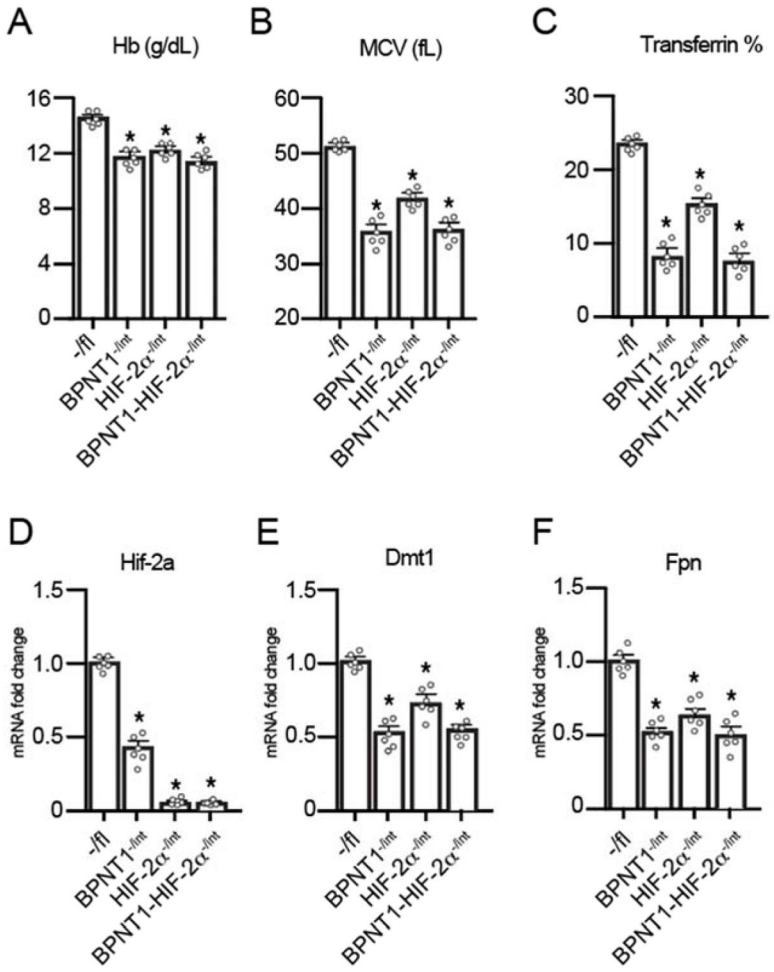

Figure 6.

Bpnt1 is epistatic to Hif-2α in the intestine. We generated Bpnt1 floxed control mice (-/fl), intestine-specific Bpnt1 knockout mice (Bpnt1$^{-/int}$), intestine-specific HIF-2α knockout mice (HIF-2α$^{-/int}$), and mice lacking both intestine-specific Bpnt1 and HIF-2α (Bpnt1-HIF-2α$^{-/int}$) and measured hemoglobin (Hb, g/dL) (A), mean corpuscular volume (MCV, fL) (B), and transferrin saturation (transferrin %) (C) in 12–16 week mice (n=6 mice per group). qRT-PCR of *Hif-2α* (D), *Dmt1* (E), and *Fpn* (F) in enterocytes (n=6) isolated from mice as described above. *Represents $p < 0.05$ by two-way ANOVA with Tukey's post-hoc test. Data are represented as mean ± SEM. There were no statistically-significant differences in any parameter tested between male and female mice.

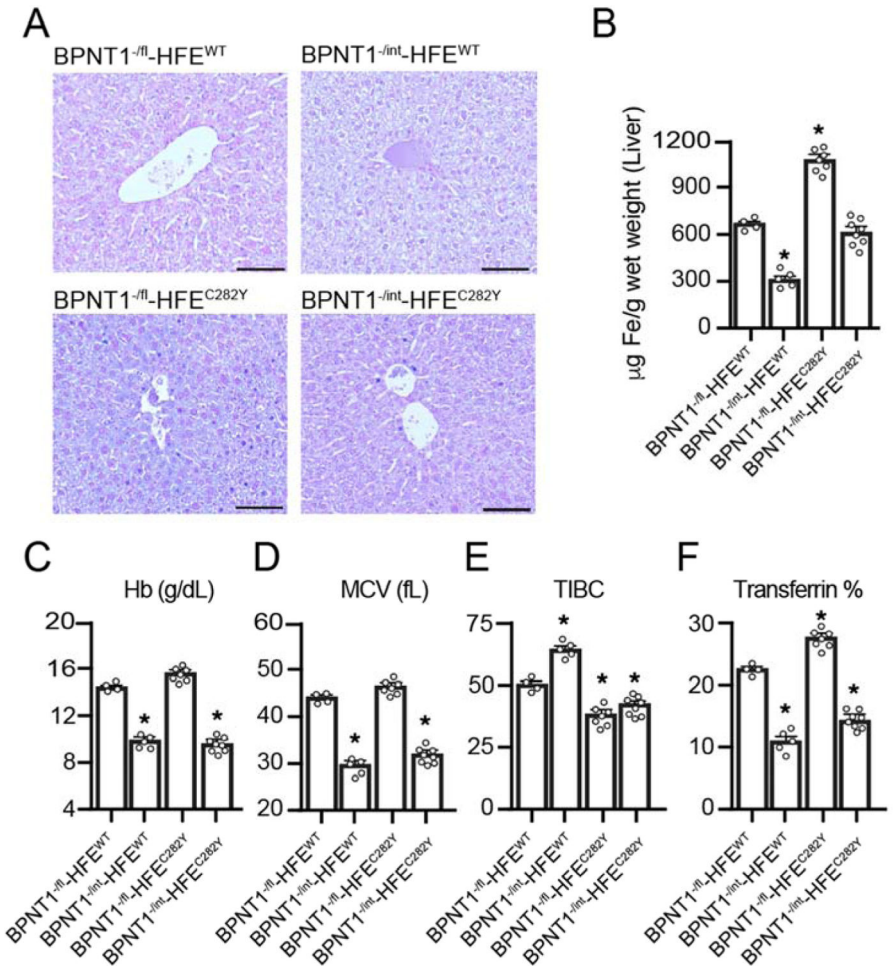

Figure 7.

Intestinal-specific deletion of Bpnt1 attenuates hepatic iron-overload in Hfe^{C282Y} homozygous mice. (A) Representative Prussian-blue staining from livers isolated from $Bpnt1^{-/fl}$, $Bpnt1^{-/int}$, Hfe^{C282Y}, and Hfe^{C282Y}- $Bpnt1^{-/int}$ mice. (B) Hepatic iron quantification from mice fed normal-chow diet as described in (A). (C) Hemoglobin (Hb, g/dL), (D) mean corpuscular volume (MCV, fL), (E) Total iron binding capacity (TIBC, the sum of serum iron and unsaturated iron binding capacity), and (F) percentage transferrin saturation (n=4–8 animals per group). *Represents $p < 0.05$ by two-way ANOVA with Tukey's post-hoc test. Data are represented as mean ± SEM. There were no statistically-significant differences in any parameter tested between male and female mice.